Fast and robust three-dimensional best path phase unwrapping algorithm

Hussein S. Abdul-Rahman,[1] Munther A. Gdeisat,[1,*] David R. Burton,[1] Michael J. Lalor,[1] Francis Lilley,[1] and Christopher J. Moore[2]

[1]General Engineering Research Institute (GERI), Liverpool John Moores University, James Parsons Building Room 114, Byrom Street, Liverpool L3 3AF, UK

[2]North West Medical Physics, Developing Technologies Section, Christie Hospital NHS Foundation Trust, Wilmslow Road, Manchester M20 4BX, UK

*Corresponding author: m.a.gdeisat@ljmu.ac.uk

Received 23 April 2007; revised 25 June 2007; accepted 13 July 2007; posted 17 July 2007 (Doc. ID 82331); published 7 September 2007

What we believe to be a novel three-dimensional (3D) phase unwrapping algorithm is proposed to unwrap 3D wrapped-phase volumes. It depends on a quality map to unwrap the most reliable voxels first and the least reliable voxels last. The technique follows a discrete unwrapping path to perform the unwrapping process. The performance of this technique was tested on both simulated and real wrapped-phase maps. And it is found to be robust and fast compared with other 3D phase unwrapping algorithms. © 2007 Optical Society of America

OCIS codes: 100.2650, 120.5050, 100.5070.

1. Introduction

Phase unwrapping has applications in many advanced imaging technologies such as optical interferometry, satellite radar interferometry (SAR), and magnetic resonance imaging (MRI), where the required data are encoded in the form of a phase distribution. The measured phase is normally wrapped between the values of $-\pi$ and π. The wrapped phase is not usable until these 2π phase discontinuities are removed, and this is accomplished by using a phase unwrapping algorithm. The actual procedure of resolving these phase jumps is carried out by either adding or subtracting integer multiples of 2π to all successive pixels after a phase discontinuity has been encountered, based on some kind of threshold mechanism.

During the last three decades, the field of two-dimensional (2D) phase unwrapping has been studied intensively and many journal papers have been published. Numerous techniques have been proposed to solve the phase unwrapping problem. These phase unwrapping techniques can be generally classified into three major categories: global error-minimization methods, residue-balancing methods, and quality-guided algorithms. A thorough review of the 2D phase unwrapping problem has been presented in the book by Ghiglia and Pritt [1].

The global error-minimization algorithms formulate the unwrapping process in terms of the minimization of a global function. All the algorithms in this class are known to be robust but are also computationally intensive. The L^p-norm and least-squares algorithms are typical examples from this category [2,3].

Residue-balancing algorithms search for residues in a wrapped-phase map and attempt to balance positive and negative residues by placing cut lines between them. The role of these cut lines is to create an unwrapping barrier and prevent the unwrapping path from going through them. The placement of a particular set of cut lines for any given wrapped-phase map is not unique, and they may be placed in many different arrangements and orientations. These algorithms are generally fast, but they are not very robust [4,5].

Quality-guided algorithms depend on a quality measure to guide the unwrapping path. The main

0003-6935/07/266623-13$15.00/0

idea of these algorithms is to unwrap the highest quality pixels first and the lowest quality pixels last to prevent error propagation during the unwrapping process [6,7]. The success or failure of these algorithms depends strongly on the production of a good quality map. The quality map can be defined to be an array of values that define the quality, or goodness, of each pixel of the given wrapped-phase data. Many 2D quality-guided algorithms have been proposed during the last few decades, and most of these algorithms tend to follow a continuous path while unwrapping the phase map. These algorithms are generally computationally efficient, and their robustness varies from one algorithm to another. One quality-guided algorithm that tends to unwrap the phase map following a discrete path was proposed by Herráez *et al.* in 2002 [8]. This algorithm is very robust and fast and has been used in constructing a robust fringe pattern analysis system for human body shape measurement [9].

Many applications produce 3D wrapped-phase volumes, such as the noncontact measurement of dynamic objects, multitemporal SAR interferometric measurements [10] and MRI [11]. A wrapped-phase volume can be visualized as a number of consecutive 2D wrapped-phase maps. A 3D phase volume consists of an array of voxels (a single element in the 3D volume that is analogous to the pixel in 2D terms). Each map can be unwrapped individually using a 2D phase unwrapping algorithm [12], or alternatively, the whole wrapped-phase volume can be unwrapped at once by using a 3D phase unwrapping algorithm.

Today, 3D phase unwrapping algorithms are of increasing interest in many applications. The 3D phase unwrapping field is still a new area of research, and only a few algorithms have been proposed so far. In a similar manner to the development of 2D phase unwrapping algorithms, 3D phase unwrapping techniques are expected to follow one of the following three approaches: a residue-balancing approach, a quality-guided approach, or a global error-minimization approach.

In 2001 Huntley proposed a 3D noise immune phase unwrapping algorithm that extended the 2D residue-balancing method into three dimensions [13]. In this method, all residues in the phase volume are identified and connected together to form singularity loops. These loops are then set as prohibited 3D barrier surfaces during the unwrapping process through which the unwrapping path must not cross, in a 3D manner that is analogous to the use of cut lines in 2D form. Huntley shows that there is only a single solution to form these singularity loops, which means that a unique solution does exist. This is in contrast to the 2D phase unwrapping algorithms where no unique solution necessarily exists.

Cusack and Papadakis proposed another robust 3D phase unwrapping algorithm that was used to unwrap MRI data [11]. This algorithm uses a quality measurement to guide the final unwrapping path. Many iterations have to be carried out in order to complete the unwrapping of the whole phase volume, as in each individual iteration only those voxels whose quality exceeds a certain threshold are unwrapped. The unwrapping of the remaining voxels is left to subsequent iterations, during which the threshold value is gradually reduced until the unwrapping process is complete.

Jenkinson proposed another 3D phase unwrapping algorithm, which tends to follow a global error-minimization approach. This technique divides the whole wrapped-phase volume into multiple regions. These regions are chosen in such a way that each region contains no phase wraps, i.e., the regions meet at and border the phase wraps but each 3D region must not contain a wrap. The individual regions are treated as single units by the algorithm. A cost function, which calculates the difference in the phase values at the interface of adjacent regions, has to then be minimized. When the cost between the two regions is at a minimum, the two regions are merged together. The process continues until only a single large region is left. This method has been designed to process 2D and 3D MRI data, but it can be extended to permit the unwrapping of N-dimensional data [14].

In this paper, the authors propose what we believe to be a novel 3D quality-guided phase unwrapping algorithm. The technique relies upon a quality measure and follows a discrete unwrapping path, unwrapping the highest quality voxels first and the lowest quality voxels last in order to prevent error propagation. The proposed technique extends Herráez's 2D algorithm into three dimensions [8]. The basic principle of the proposed technique has been previously presented at least in outline and compared with its 2D counterpart and other 3D algorithms [15,16]. We seek to present the algorithm in a complete and rigorous form and demonstrate its application to simulated test data and real applications. This algorithm is surprisingly robust, as we will demonstrate.

In Section 2 the proposed algorithm will be explained in detail. Subsection 2.A explains how to measure the quality of a voxel in the 3D phase volume, and Subsection 2.B explains how the unwrapping path is determined. In Section 3, simulated and real results are shown and are also compared with the Huntley and Cusack algorithms in terms of robustness, reliability, and execution time.

2. Algorithm

In a similar manner to other quality-guided phase unwrapping algorithms, two main issues will determine the behavior of the proposed algorithm: the choice of the quality function that guides the unwrapping path and the design of the unwrapping path that minimizes error propagation during the unwrapping procedure. These two main issues are discussed and explained in the following subsections from the perspective of the proposed algorithm.

A. Three-Dimensional Quality Maps

Two-dimensional quality-guided phase unwrapping algorithms use different criteria to determine the

quality of each individual pixel in the phase map. Quality maps that are based upon pseudocorrelation, phase derivative variance, the maximum gradient, and the second difference of the input wrapped phase, are among the most well-known methods for producing 2D quality maps. These have been integrated into many phase unwrapping algorithms and have produced very robust results [1].

The quality maps mentioned previously are here extended into 3D form in order to suit the proposed algorithm. The method for calculation of each quality map in the 3D case is explained in Subsections 2.A.1–2.A.4.

1. Three-Dimensional Pseudocorrelation Quality Map

To calculate the 3D pseudocorrelation quality map for a voxel, $v(m, n, l)$, in a phase volume, using a $3 \times 3 \times 3$ cube, the summation of cosines and sines of the values of the voxel and its 26 neighbors are calculated using the equation:

$$Q_{m,n,l} = \frac{1}{27} * \left(\sum (\cos(\psi_{i,j,k}))^2 + \sum (\sin(\psi_{i,j,k}))^2\right)^{1/2}, \quad (1)$$

where $\psi_{m,n,l}$ is the wrapped-phase value of the voxel $v(m, n, l)$. i, j, k represent the neighbors's indices of the voxel $v(m, n, l)$ in a $3 \times 3 \times 3$ cube.

2. Three-Dimensional Phase Derivative Variance Quality Map

The phase derivative variance measures the statistical variance of the phase derivative. Actually, the phase derivative variance indicates a measure of the badness rather than the goodness of the phase data. The calculation of the phase derivative variance for a voxel $v(m, n, l)$ in the volume using a $3 \times 3 \times 3$ cube is defined by the equation:

$$V_{m,n,l} = \frac{1}{27} * \left(\sqrt{\sum \left(\Delta_{i,j,k}{}^{x} - \overline{\Delta_{i,j,k}{}^{x}}\right)^2} + \sqrt{\sum \left(\Delta_{i,j,k}{}^{y} - \overline{\Delta_{i,j,k}{}^{y}}\right)^2} + \sqrt{\sum \left(\Delta_{i,j,k}{}^{z} - \overline{\Delta_{i,j,k}{}^{z}}\right)^2}\right), \quad (2)$$

where Δ^x, Δ^y, and Δ^z are the wrapped-phase gradients in the x, y, and z directions, respectively. $\overline{\Delta^x}$, $\overline{\Delta^y}$, and $\overline{\Delta^z}$ are the mean of the values in a $3 \times 3 \times 3$ cube in Δ^x, Δ^y, and Δ^z, respectively. i, j, k are neighbors's indices of the voxel $v(m, n, l)$ in a $3 \times 3 \times 3$ cube. Δ^x, Δ^y, and Δ^z are 3D arrays, and each one has the same dimensions as the wrapped-phase volume. These three arrays are defined by Eq. (3):

$$\Delta_{i,j,k}{}^{x} = \gamma[\psi_{i+1,j,k} - \psi_{i,j,k}],$$
$$\Delta_{i,j,k}{}^{y} = \gamma[\psi_{i,j+1,k} - \psi_{i,j,k}],$$
$$\Delta_{i,j,k}{}^{z} = \gamma[\psi_{i,j,k+1} - \psi_{i,j,k}], \quad (3)$$

where γ defines a wrapping operator that will wrap all values of its argument into the range $[-\pi, \pi]$ by adding or subtracting an integer number of 2π rad to its argument, i.e., $y = \gamma(x)$ is equivalent to $y = \arctan(\sin(x)/\cos(x))$.

Finally, the quality of the voxel is defined to be the reciprocal of the variance as described by the equation:

$$Q_{m,n,l} = \frac{1}{V_{m,n,l}}. \quad (4)$$

3. Three-Dimensional Maximum Gradient Quality Map

The maximum phase gradient measures the magnitude of the largest phase gradient, i.e., the local wrapped-phase difference. The maximum gradient of the voxel $v(m, n, l)$ can be calculated by finding the maximum gradient of the voxel and its 26 neighbors in the x, y, or z directions, as described in Eq. (5). Similar to the case with the phase derivative variance quality map, the maximum gradient method indicates the badness rather than the goodness of the phase data, so the quality is calculated using the reciprocal of the phase gradient:

$$M_{m,n,l} = \max\{\max\{|\Delta_{i,j,k}{}^{x}|\}, \max\{|\Delta_{i,j,k}{}^{y}|\}, \max\{|\Delta_{i,j,k}{}^{z}|\}\}. \quad (5)$$

4. Three-Dimensional Second Difference Quality Map

To calculate the quality of a voxel using the second difference algorithm, the second differences between the voxel and its neighbors are first calculated using the equation:

$$SD_{i,j,k} = \sqrt{H^2(i, j, k) + V^2(i, j, k) + N^2(i, j, k) + \sum_{n=1}^{10} D_n{}^2(i, j, k)}, \quad (6)$$

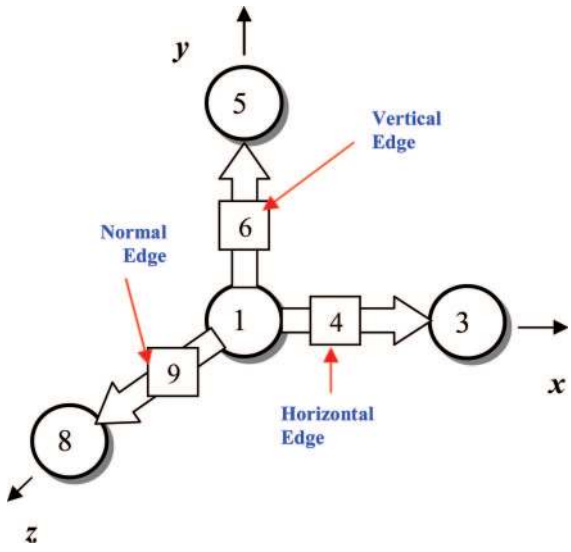

Fig. 1. (Color online) Definition of the edges and their qualities.

where

$$H(i,j,k) = \gamma[\varphi(i-1,j,k) - \varphi(i,j,k)] - \gamma[\varphi(i,j,k) - \varphi(i+1,j,k)],$$

$$V(i,j,k) = \gamma[\varphi(i,j-1,k) - \varphi(i,j,k)] - \gamma[\varphi(i,j,k) - \varphi(i,j+1,k)],$$

$$N(i,j,k) = \gamma[\varphi(i,j,k-1) - \varphi(i,j,k)] - \gamma[\varphi(i,j,k) - \varphi(i,j,k+1)],$$

$$D_1(i,j,k) = \gamma[\varphi(i-1,j-1,k) - \varphi(i,j,k)] - \gamma[\varphi(i,j,k) - \varphi(i+1,j+1,k)],$$

$$D_2(i,j,k) = \gamma[\varphi(i+1,j-1,k) - \varphi(i,j,k)] - \gamma[\varphi(i,j,k) - \varphi(i-1,j+1,k)],$$

$$D_3(i,j,k) = \gamma[\varphi(i-1,j-1,k-1) - \varphi(i,j,k)] - \gamma[\varphi(i,j,k) - \varphi(i+1,j+1,k+1)],$$

$$D_4(i,j,k) = \gamma[\varphi(i,j-1,k-1) - \varphi(i,j,k)] - \gamma[\varphi(i,j,k) - \varphi(i,j+1,k+1)],$$

$$D_5(i,j,k) = \gamma[\varphi(i+1,j-1,k-1) - \varphi(i,j,k)] - \gamma[\varphi(i,j,k) - \varphi(i-1,j+1,k+1)],$$

$$D_6(i,j,k) = \gamma[\varphi(i-1,j,k-1) - \varphi(i,j,k)] - \gamma[\varphi(i,j,k) - \varphi(i+1,j,k+1)],$$

$$D_7(i,j,k) = \gamma[\varphi(i-1,j+1,k-1) - \varphi(i,j,k)] - \gamma[\varphi(i,j,k) - \varphi(i+1,j-1,k+1)],$$

$$D_8(i,j,k) = \gamma[\varphi(i+1,j,k-1) - \varphi(i,j,k)] - \gamma[\varphi(i,j,k) - \varphi(i-1,j,k+1)],$$

$$D_9(i,j,k) = \gamma[\varphi(i,j+1,k-1) - \varphi(i,j,k)] - \gamma[\varphi(i,j,k) - \varphi(i,j-1,k+1)],$$

$$D_{10}(i,j,k) = \gamma[\varphi(i+1,j+1,k-1) - \varphi(i,j,k)] - \gamma[\varphi(i,j,k) - \varphi(i-1,j-1,k+1)]. \quad (7)$$

H, V, and N are the horizontal, vertical, and normal second differences, respectively. D_n is the nth diagonal second difference. The second difference also gives a measure of the badness of each voxel, so the quality of each voxel is given by the reciprocal of the second difference value.

The second difference quality map can be calculated without the requirement for using the diagonal differences. This reduces computational complexity,

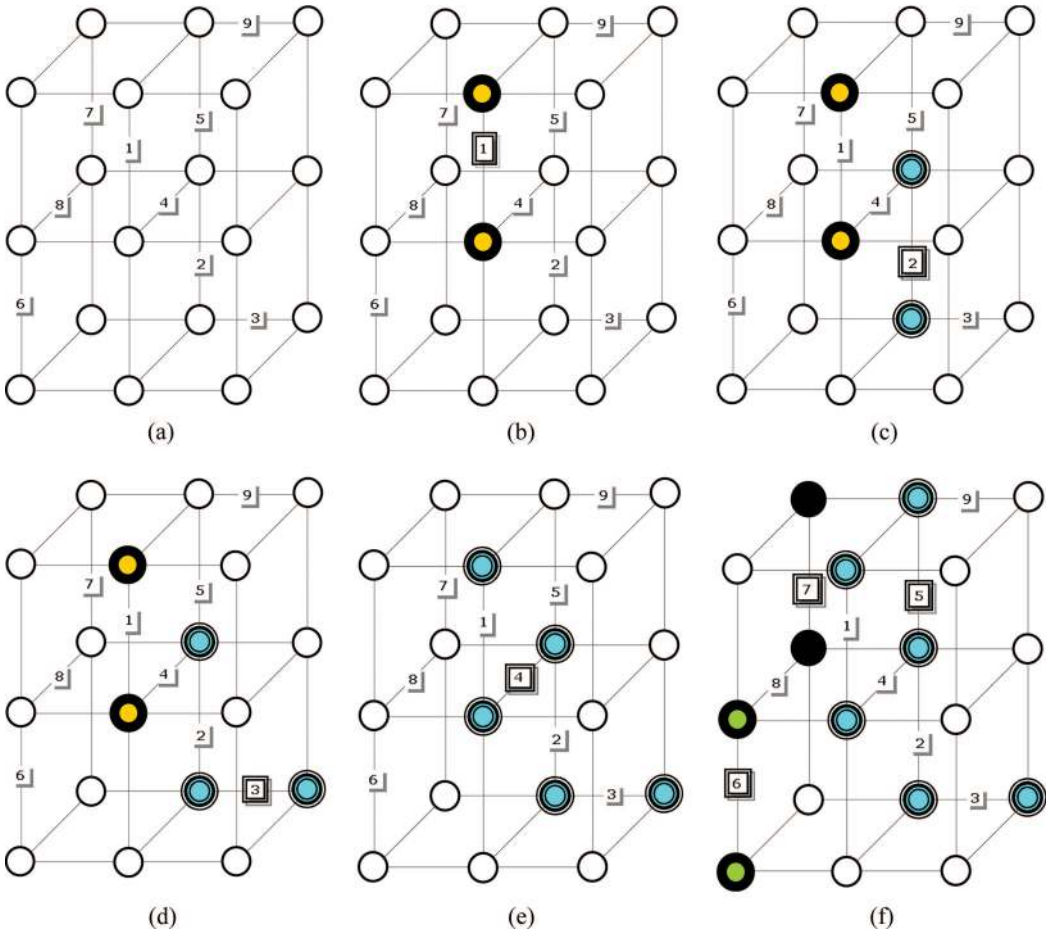

Fig. 2. (Color online) Demonstration of the unwrapping path of the proposed algorithm.

but it may also reduce the robustness of the algorithm.

B. Unwrapping Path

Most quality-guided phase unwrapping algorithms rely on the quality of the voxels themselves to guide the unwrapping path. The unwrapping path for the proposed algorithm relies upon the quality of the edges as an intermediate stage, rather than relying on the quality of the voxels.

An edge is an intersection of two voxels that are connected in the x, y, or z directions. Edges can be classified as vertical, horizontal, or normal edges as shown in Fig. 1. In this figure, the voxels are represented by circles, and the edges are represented by squares. The quality of an edge is defined as the summation of the individual quality values of the two voxels that are connected together by the edge. This is shown in Fig. 1, where the numbers inside the circles represent values for individual voxel quality, whereas the numbers inside the squares represent quality values for edges. The proposed algorithm sets the edge quality value to zero for an edge that connects a border voxel with another voxel in the phase volume.

In the proposed algorithm the unwrapping path is determined by the quality values of the edges. The definition of the unwrapping path is relatively simple. All the edges are stored in an array and sorted in terms of their edge quality values. Those edges with higher qualities are resolved first, in a manner that will be explained later. The construction of the unwrapping path is similar to the discrete unwrapping path described by Herráez *et al.* [8] but is extended into three dimensions.

Figures 2(a)–2(f) illustrate the principle of the proposed algorithm. The volume shown in Fig. 2(a) is a wrapped-phase volume that needs to be unwrapped. The edges's quality values have already been sorted, and their order is shown in the figure. The integer numbers represent the processing order of the edges in the sorted array. The edge that has the order 1 is the one that had the largest quality value and will be processed first, then the edge with the second-highest quality value, denoted as having an integer order value of 2 is processed next, and so on.

Initially all voxels are considered as not belonging to any group, which is represented by the white circles in Fig. 2(a). Both voxels forming the edge with order 1 in Fig. 2(a) are unwrapped first with respect to each other, and both voxels are joined together to form a single group, as illustrated in Fig 2(b). After processing this edge, the algorithm will search for the next edge to be processed, which is the edge with order 2 as shown in Fig. 2(b). Because both voxels forming edge 2 do not belong to any group, they are unwrapped with respect to each other and form a new group as illustrated in Fig. 2(c).

The voxels forming the edge with order 3 in Fig. 2(c) are to be processed during this stage. We can see that

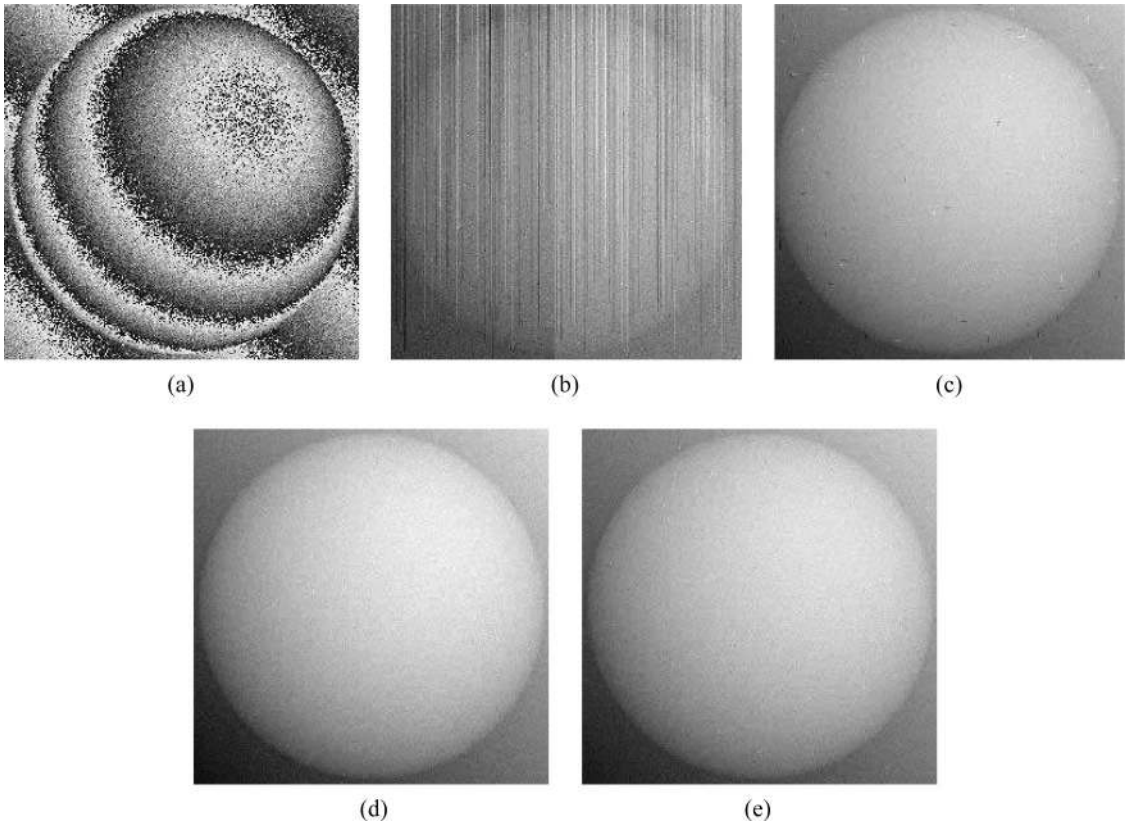

Fig. 3. Results for the last frame ($t = 99$) of the simulated spherical object. (a) Wrapped phase, the unwrapped phase using the (b) flood-fill algorithm, (c) Cusack algorithm, (d) Huntley algorithm, and (e) proposed algorithm.

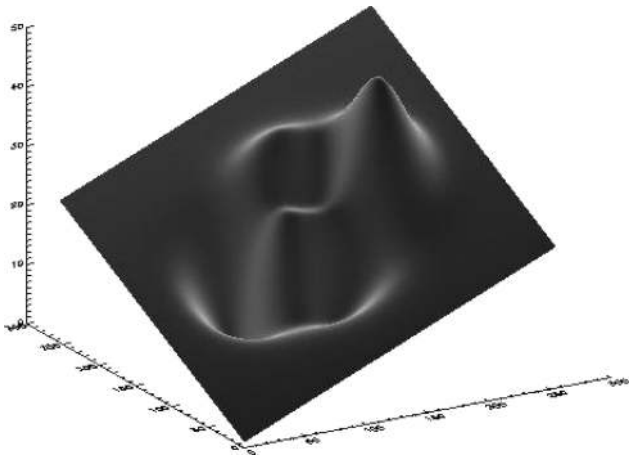

Fig. 4. Three-dimensional representation for the first frame ($t = 0$) of the simulated steep surface object.

one of these voxels has its own group, but the other voxel does not belong to any group. The ungrouped voxel is unwrapped with respect to the grouped voxel, and it is set to be a member of this group as shown in Fig. 2(d).

Edge number 4 in Fig. 2(d) connects two grouped voxels, so in this case the group of fewer members is unwrapped with respect to the group with more members, by either adding or subtracting multiple integers of 2π to each voxel in the group. Then both groups merge into a single group as illustrated in Fig. 2(e).

The algorithm will continue this process of forming new groups, joining ungrouped voxels to the other existing groups and merging groups together until all of the voxels have been unwrapped and become members of one large group. Figure 2(f) shows the formation of new groups while the unwrapping process is being carried out. Note that unwrapping a voxel or a group of voxels with respect to another group may require the addition or subtraction of multiples of 2π.

The proposed algorithm can be summarized in the following steps:

1. Determine the qualities of all voxels.
2. Calculate the horizontal, vertical, and normal edges's qualities and set the qualities of the edges that are connected with the borders to zero in order to be processed last.
3. Sort all of the edges according to their qualities in descending order.
4. Unwrap voxels according to the edges qualities, so that the voxels that form the highest quality edges are unwrapped first according to the following rules:
   A. If both voxels do not belong to any group and have not been unwrapped before, the voxels are

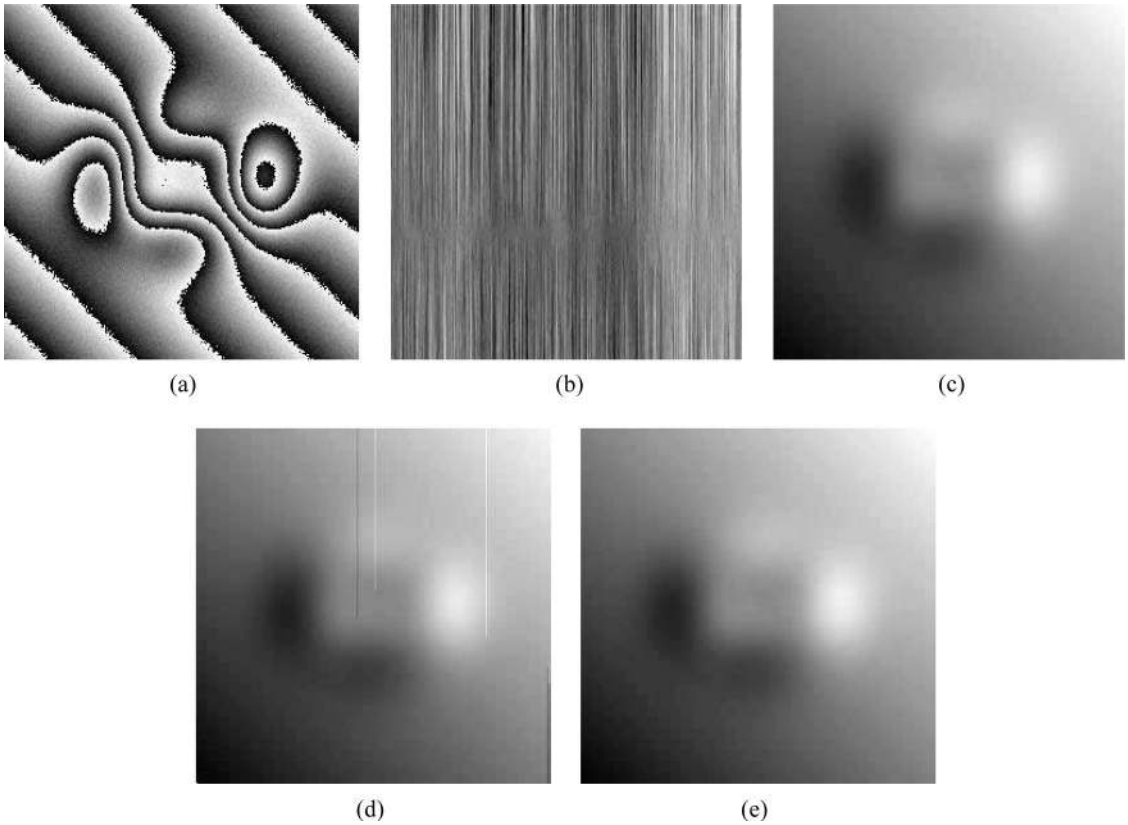

Fig. 5. Results for the first frame ($t = 0$) of the simulated steep surface object. (a) Wrapped phase, the unwrapped phase using the (b) flood-fill algorithm, (c) Cusack algorithm, (d) Huntley algorithm, and (e) proposed algorithm.

unwrapped with respect to each other and gathered into a single group.

B. If one of the voxels has been processed before and belongs to a group, but the other has not, then the voxel that has not been processed before is unwrapped with respect to the other voxels in the group and now joins this group.

C. If both voxels have been processed before and both belong to different groups, then the two groups are unwrapped with respect to each other. The smaller group is unwrapped with respect to the larger group. Then the two groups are joined together to construct a single group.

3. Results

To evaluate the performance of the proposed algorithm, two sets of wrapped-phase volumes have been used: computer-generated and real wrapped-phase volumes. Both types of phase volumes have been unwrapped using the proposed technique. The results of this phase unwrapping algorithm are then compared with other existing 3D phase unwrapping algorithms.

A. Computer Simulation Results

The proposed algorithm has been tested using many simulated computer-generated objects. The results of the proposed algorithm are compared with two well-known 3D phase unwrapping algorithms. Both algorithms are considered to be state of the art in 3D phase unwrapping, and they have been used previously in many applications and have proven their robustness and high performance in many applications. The first algorithm is the 3D phase unwrapping algorithm proposed by Cusack and Papadakis, and it is now in use for the efficient unwrapping of MRI phase volumes [12]. The second comparative technique is the 3D noise immune phase unwrapping algorithm proposed by Huntley [13].

The first computer-generated object is a simple growing sphere whose radius is increasing with time, i.e., with the frame number. The sphere grows from the minimum to the maximum radius in 100 frames, each frame consisting of 256×256 pixels. Then Gaussian noise with zero mean and a standard deviation of 0.75 is added to each frame of the $256 \times 256 \times 100$ volume. The whole volume is subsequently wrapped between $-\pi$ to π using the arctangent function and scaled between black and white for display purposes. The color white represents the maximum height of the object, and the color black represents its minimum height.

Figure 3 shows the wrapped-phase and unwrapped-phase maps for the last frame ($t = 99$) of this sphere. As seen in the figure, the 3D flood-fill phase unwrapping algorithm completely fails to unwrap this phase volume, due to its high noise levels, as shown in Fig 3(a). On the other hand, the proposed algorithm and the Huntley algorithm successfully unwrap this

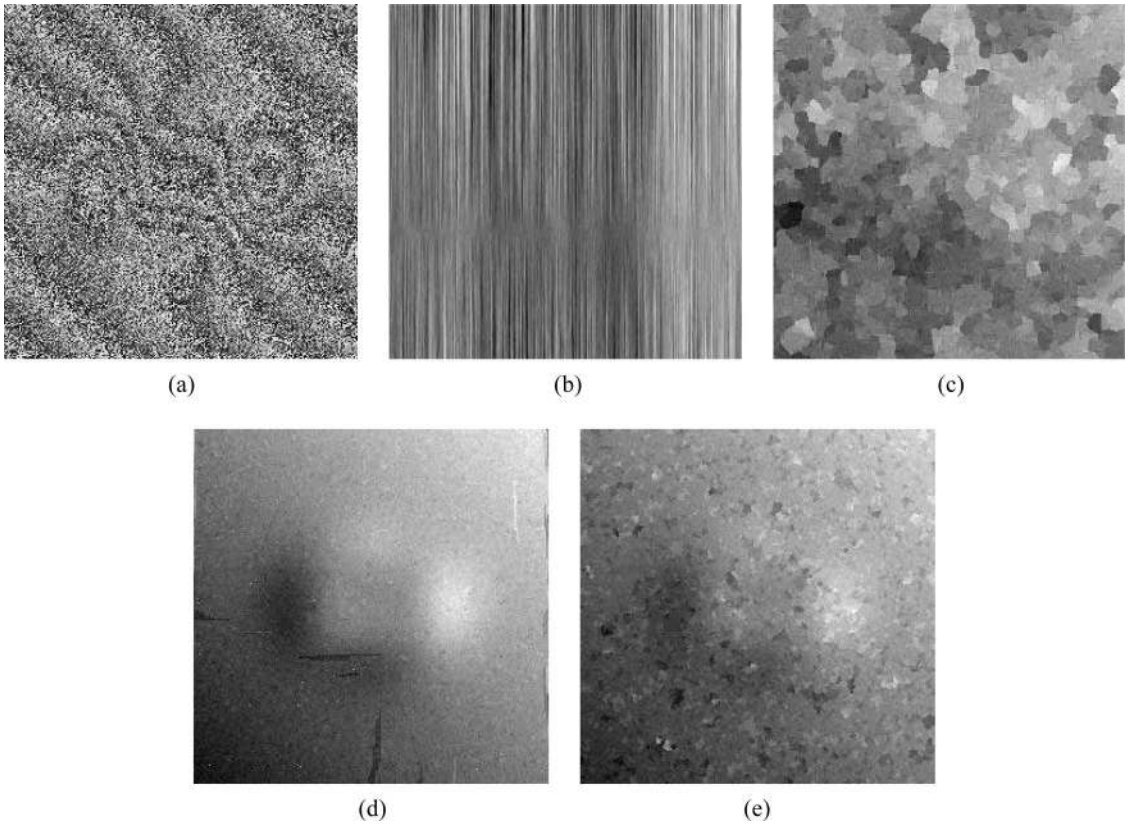

Fig. 6. Results for the last frame ($t = 99$) of the simulated steep surface object. (a) Wrapped phase, the unwrapped phase using the (b) flood-fill algorithm, (c) Cusack algorithm, (d) Huntley algorithm, and (e) proposed algorithm.

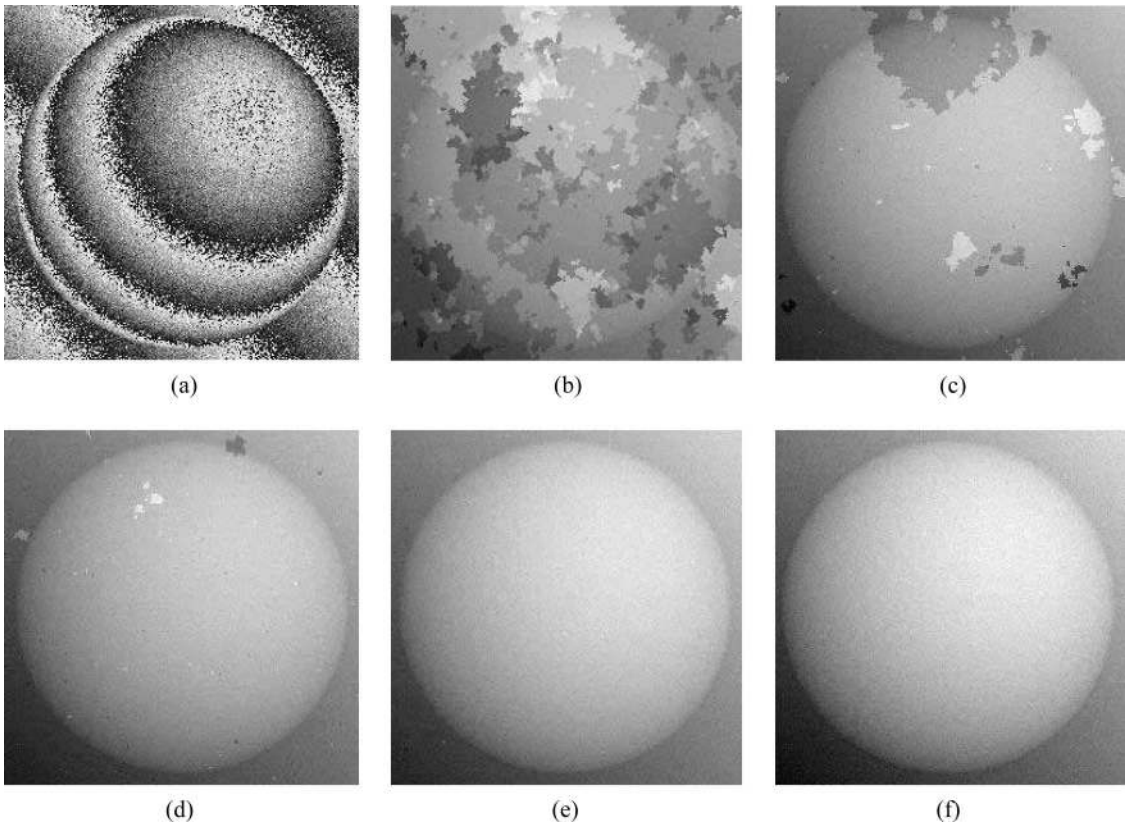

Fig. 7. Effect of quality map on the unwrapping path for a simulated spherical object, (a) wrapped-phase map at frame number 75 ($t = 75$), unwrapped-phase map for the same frame resulting from using: (b) pseudocorrelation, (c) maximum gradient, (d) phase derivative variance, (e) second difference using 26 neighbors, and (f) second difference using only six orthogonal neighbors.

wrapped-phase volume and deliver excellent results, as shown in Figs. 3(d) and 3(e), respectively. Figure 3(c) shows the unwrapped-phase map for this frame resulting from the use of the Cusack algorithm. The Cusack algorithm gives a very good result but does not perform as well as the Huntley algorithm and the proposed algorithm.

The second simulated object is a complex surface with steep sided features, whose height is increasing with time, as described in Eq. (9). The object moves from its minimum height to the maximum height in 100 frames, each frame again consisting of 256 × 256 pixels:

$$\begin{aligned} z_{i,j,t} = {} & 6.12\left[(1-{x_1}^2)\exp\left(-{x_1}^2-(y_1+1)^2\right)\right] \\ & -20.6\left[\left(\frac{x_1}{5}-{x_1}^3-{y_1}^5\right)\exp\left(-{x_1}^2-{y_1}^2\right)\right] \\ & -0.68\left[\exp\left(-(x_1+1)^2-{y_1}^2\right)\right]+0.1(x_2+y_2) \\ & +(0.01t), \end{aligned} \tag{9}$$

where x_1 and y_1 are defined in the range of $[-3.5, 3.5]$ and x_2 and y_2 are defined in the range $[0, 255]$. $z_{i,j,t}$ is the height of the pixel (i, j) at time t (actually, t represents the frame number). The height difference between two successive frames is 0.01 units. A 3D representation of this object at ($t = 0$) is shown in Fig. 4.

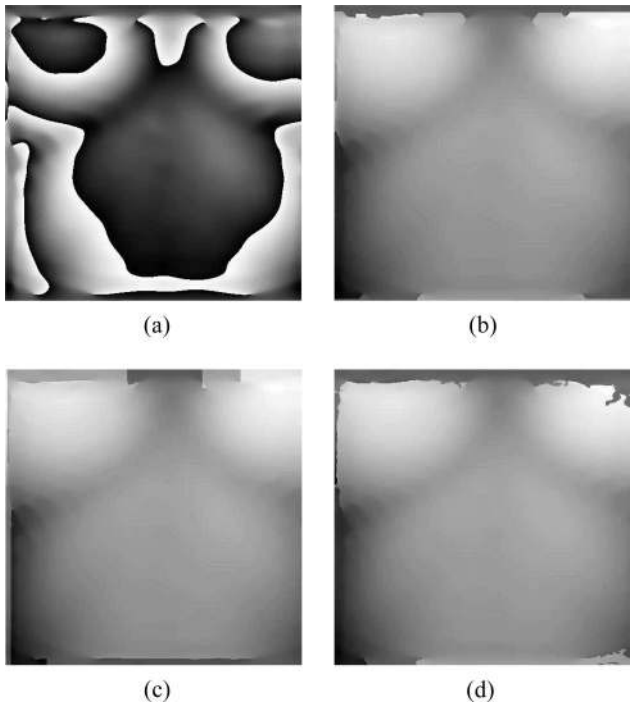

Fig. 8. Results of frame 25 of the mannequin's chest: (a) wrapped phase, (b) unwrapped phase using the (b) Cusack algorithm, (c) Huntley algorithm, and (d) proposed algorithm.

Gaussian noise is added to the object's 256 × 256 × 100 frames as follows:

$$Noise_{(at\ frame\ t)} = Noise_{(at\ frame\ t-1)} + 256 \times 256\ Gaussian\ noise_{(mean=0,\sigma=0.165)}.$$

Supposing that the noise at frame $t = -1$ is equal to zero, where σ is the standard deviation of the noise distribution. This means that for this example the noise levels are not constant for each frame, as they were in the previous case, but instead the noise increases from a minimum in the first frame to a maximum level in the final frame of the sequence. The whole volume is subsequently wrapped between the values $-\pi$ to π using the arctangent function and scaled between black and white for display purposes. The color white represents the maximum height of the object and the color black represents its minimum height.

As shown in Fig. 5, all of the algorithms successfully unwrap the first frame ($t = 0$) where the noise is minimum, except for the 3D flood-fill algorithm, which completely fails due to the high noise levels that exist in the phase map. The proposed algorithm and the Cusack algorithm give very smooth results, as shown in Figs. 5(c) and 5(e), respectively. The Huntley algorithm gives the worst results for this particular frame, and both the Cusack algorithm and the proposed algorithm give better output.

As the amount of noise increases accumulatively from frame to frame, unwrapping the higher frames becomes very difficult. Figure 6 shows the results from all algorithms at the final frame ($t = 99$), where the noise is at a maximum. Figure 6(a) shows the wrapped-phase map at this frame, clearly the

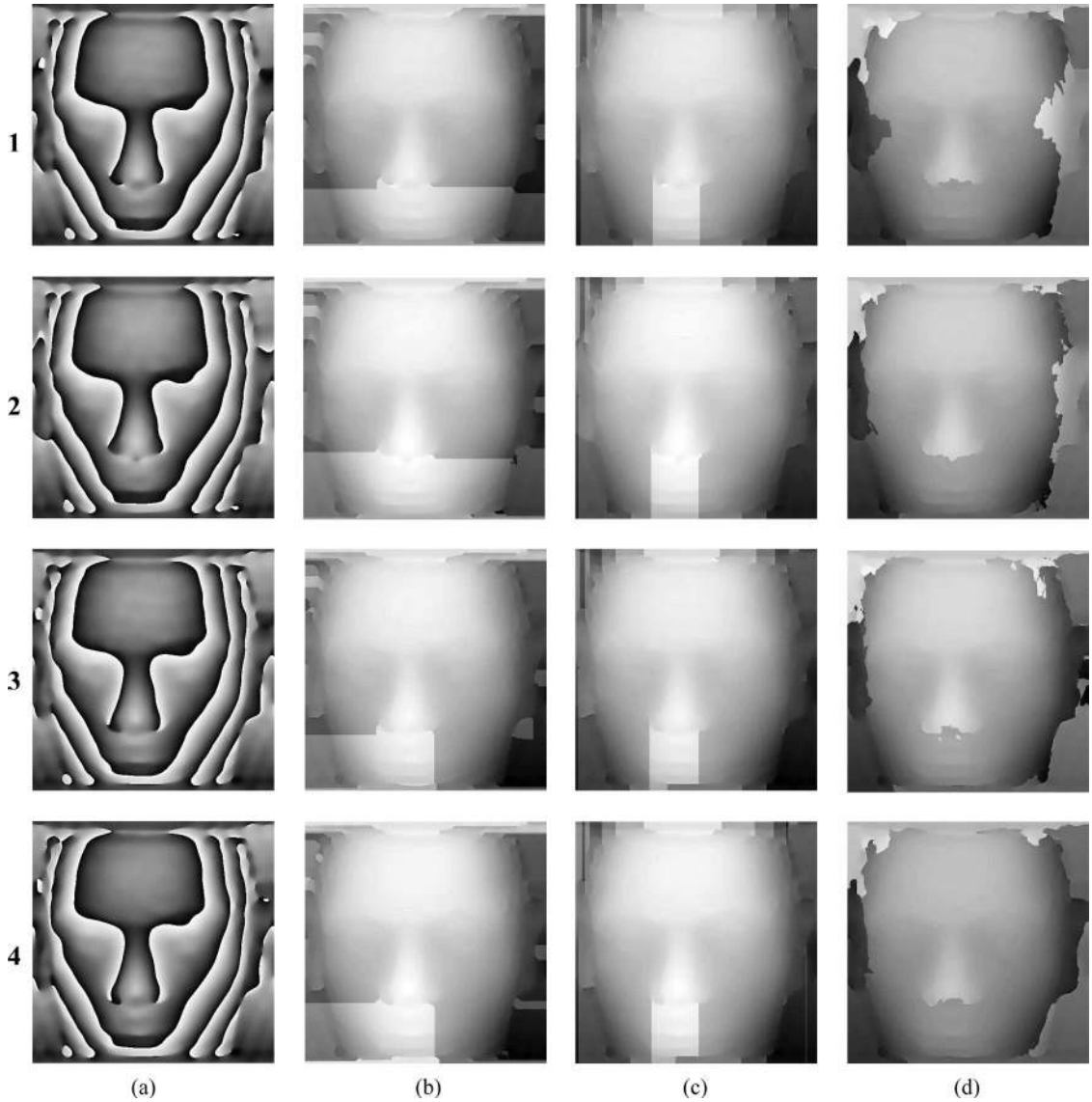

Fig. 9. Results for frames 0, 25, 35, and 49 of the RANDO dummy's face shown in rows 1, 2, 3, and 4, respectively, (column a) represents the wrapped-phase maps for these particular frames, the unwrapped-phase maps of these frames resulting from using the (column b) Cusack algorithm, (column c) Huntley algorithm, and (column d) proposed algorithm.

amount of noise in this frame is very large, and it will undoubtedly be a very difficult image to unwrap. Figure 6(b) shows the results of the 3D flood-fill algorithm. The unwrapped-phase map resulting from the application of the Cusack algorithm is shown in Fig. 6(c). As shown in Fig. 6(c), the Cusack algorithm completely fails in this frame, and the result was very poor. Figure 6(d) shows the results of the Huntley 3D noise immune technique. This algorithm succeeds in unwrapping this frame and gives an excellent result. The output of the proposed technique at this frame is shown in Fig. 6(e). The proposed algorithm outperforms the Cusack algorithm, and indeed it gives a good result for such a large level of noise. On the other hand, it can easily be seen that the proposed algorithm did not give as good a result as the 3D noise immune algorithm, which illustrates the robustness of the noise immune technique in noisy conditions.

Figures 5 and 6 show that the Huntley algorithm was not capable of isolating all the noisy regions in the wrapped phase volumes. Despite the fact that all singularity loops have been identified, there are still some errors propagate to affect less noisy regions as seen in Fig. 5.

Choosing a different quality map leads the proposed algorithm into a different unwrapping path and gives different results. Figure 7 shows the effect of choosing different quality maps when unwrapping the spherical object that was described earlier. This figure shows the unwrapped-phase maps of frame number 75 ($t = 75$) taken from that wrapped-phase volume. The results of pseudocorrelation, maximum gradient, phase derivative variance, the second difference method using only six neighbors and the second difference method using all 26 neighbors, are shown in Fig. 7.

B. Experimental Results

The proposed algorithm has also been tested experimentally in that it has been used to unwrap several 3D wrapped-phase volumes that have resulted from the analysis of real fringe patterns projected onto the surface of dynamically moving objects. A video sequence of the moving modulated fringe patterns was captured over the measurement period for each object. This video sequence was subsequently analyzed frame by frame, using a 2D Fourier fringe analysis algorithm, in order to produce a stack of 2D wrapped-phase maps. Note that the extraction of wrapped-phase has not been optimized here and the wrapped-phase volumes are presented merely as vehicles for the testing of the unwrapping algorithm. This stack of 2D wrapped-phase maps can then be considered to form a 3D wrapped-phase volume, and it is this that has been unwrapped using the proposed algorithm.

The practical application that the phase unwrapping algorithm has been tested on is that of dynamic human body measurement in radiotherapy treatment. This is an exacting application of 3D measurement technology, which requires accurate dynamic measurements to be made in conditions that are far from ideal.

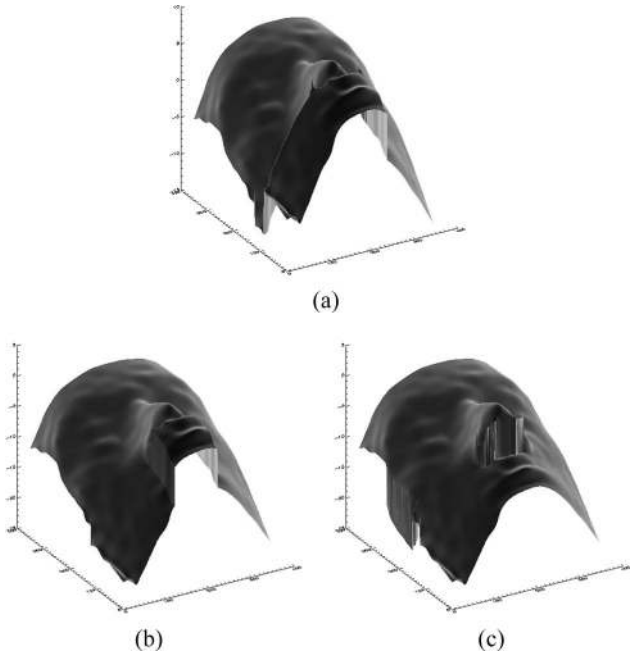

Fig. 10. Three-dimensional view for the unwrapped-phase maps for frame 49 of the RANDO dummy's face using the (a) Cusack algorithm, (b) Huntley algorithm, and (c) proposed algorithm.

We have used three wrapped-phase volumes to show the performance of the proposed algorithm in unwrapping real wrapped-phase volumes. The first two examples are taken from experiments carried out in the laboratory, simulating patient motion, and the third example is from a real clinical setting. Each

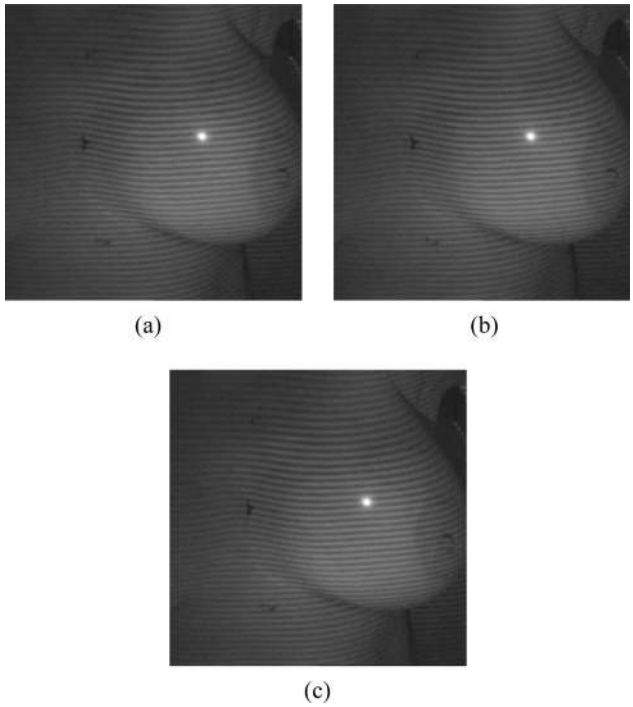

Fig. 11. Three different frames of fringe patterns for a patient undergoing radiotherapy treatment for breast cancer. (a) Frame 0, (b) frame (15), and (c) frame (24).

wrapped-phase volume consists of 50 frames with 512×512 pixels in each frame. The first wrapped-phase volume has been obtained from analyzing the chest–thorax region of a mannequin that has been manually raised and lowered in the mid-sagittal plane with a dorsal–ventral motion simulating respiration. The second wrapped-phase volume has been obtained by analyzing the face of a RANDO Phantom,

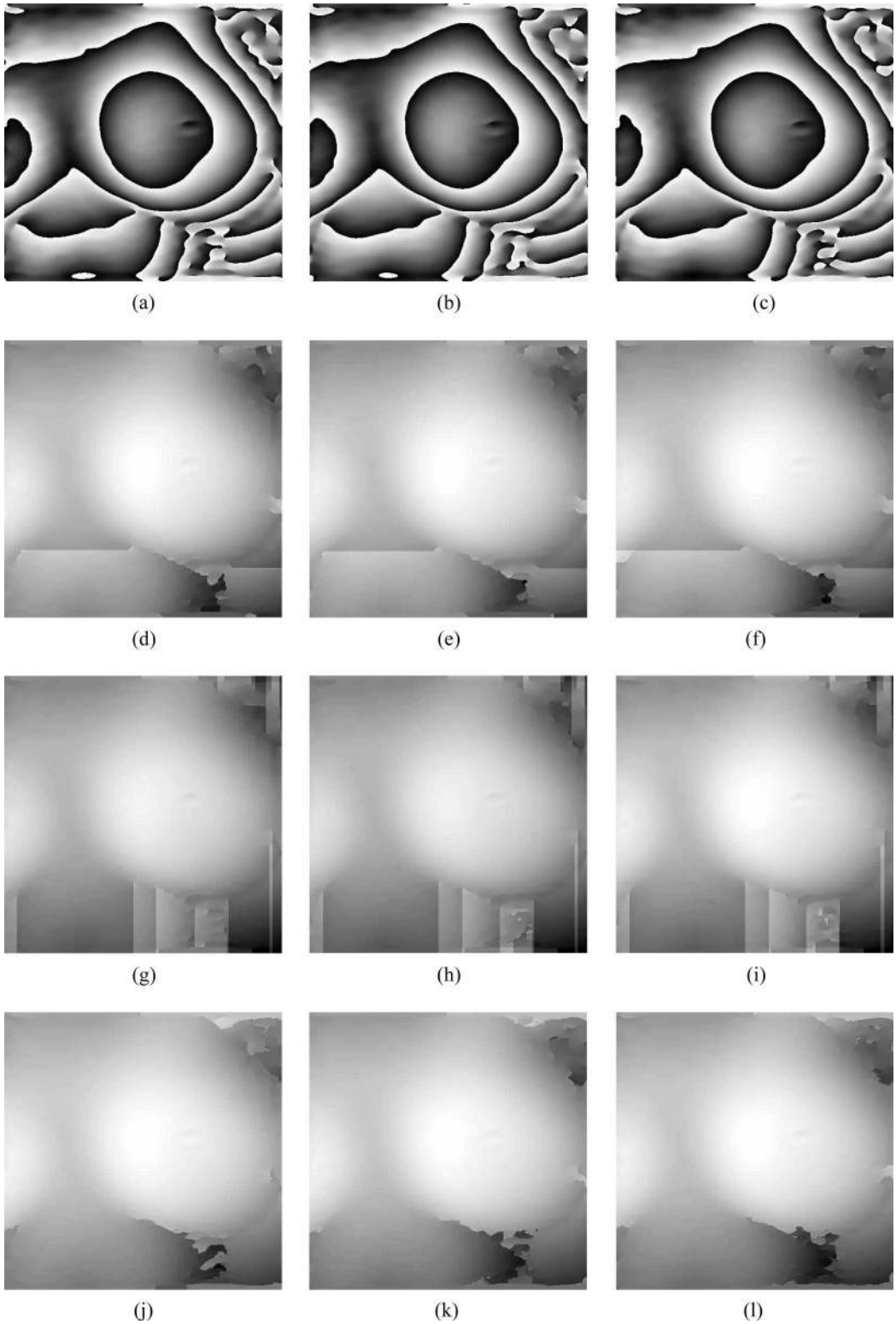

Fig. 12. Results showing a region from a female human thorax, taken from a real clinical patient undergoing treatment for breast cancer. Wrapped-phase images of frames 0, 15, and 24 are shown in (a), (b), and (c), respectively. The unwrapped-phase for those frames are shown underneath, using the (d)–(f) Cusack algorithm, (g)–(i) Huntley algorithm, and (j)–(l) proposed algorithm.

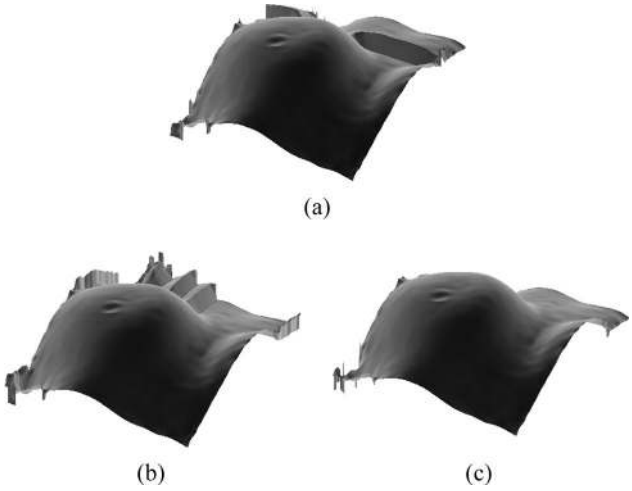

Fig. 13. Three-dimensional view for the unwrapped-phase maps for frame 24, showing a clinical patient's breast using the (a) Cusack algorithm, (b) Huntley algorithm, and (c) proposed algorithm.

a synthetic human used in radiotherapy calibration, undergoing similar manual motion in a laboratory setting. The third and final wrapped-phase volume is actual patient data acquired in a real medical clinical trial in a radiotherapy treatment room, exhibiting respiratory and ordinary levels of expected patient movement for a patient who is actually undergoing treatment for breast cancer.

Figure 8 shows frame number 25 of the mannequin's chest. Figure 8(a) shows the wrapped-phase map at that particular frame. The unwrapped-phase maps for this frame resulting from the Cusack, the Huntley, and the proposed algorithms are shown in Figs. 8(b), 8(c), and 8(d), respectively. Clearly, all algorithms successfully unwrap this wrapped-phase volume and they give satisfactory results.

Figure 9 shows four different frames of the wrapped-phase volume resulting from measuring the radiotherapy RANDO Phantom dummy's face. The first column in the figure shows the wrapped-phase maps for frames number 0, 25, 35, and 49, respectively. The second column in the figure shows the unwrapped-phase maps resulting from the Cusack algorithm. The unwrapped-phase maps resulting from the Huntley algorithm are shown in the third column. The final column shows the results of the proposed algorithm.

Figure 9 shows that the proposed algorithm was capable of unwrapping the unreliable regions last to prevent error propagation. The Cusack and Huntley algorithms create separate regions in unwrapping the dummy's face. These discontinuities in the unwrapped phase volume are the result of the failure of both phase unwrapping algorithms. On the contrary, the unwrapped-phase volume produced by the proposed algorithm is smooth and does not contain any discontinuities. Clearly, for this particular example the proposed algorithm outperforms the other two algorithms and successfully unwraps the volume whereas the other algorithms failed. A 3D representation of the unwrapped-phase map for the last frame is shown in Fig. 10.

Figure 11 shows frames 0, 15, and 24 taken from a video sequence of a patient undergoing radiotherapy treatment for breast cancer, displaying the real source fringe patterns that are to be analyzed. The patient has to be still during the treatment, so there is not much difference in fringe patterns shown in the figure. The top row of images presented in Fig. 12 shows the processed wrapped-phase maps corresponding to the three fringe patterns shown in Fig. 11. The second row shows the unwrapping results associated with these respective frames using the Cusack algorithm. The third row shows similar results for the Huntley algorithm and the bottom row for the proposed algorithm. It can be seen that the Huntley and Cusack algorithms failed again to unwrap this volume successfully as they create discontinuous surfaces on the unwrapped-phase volume; it can also been seen that the proposed algorithm outperforms the existing algorithms for this example application as it produce a smooth unwrapped phase volume without discontinuities. This may be seen more clearly in the 3D isometric plots for frame 24 as shown in Fig. 13.

The proposed algorithm and the 3D noise immune algorithm have been implemented using the C programming language and compiled using an Intel 9.1 compiler. For comparison purposes, a precompiled executable program for the Cusack algorithm was obtained from Cusack himself. These algorithms have been executed on a PC with a Pentium 4 processor running at a 3.2 GHz clock speed. The memory of the PC is 4 Gbytes of RAM. The execution time of the proposed algorithm varies from volume to volume and depends on the particular phase distribution being analyzed. The execution times for simulated and real volumes discussed earlier for each algorithm are listed in Table 1.

Table 1. Execution Times in Seconds for the Proposed Algorithm, the Cusack Algorithm, and the 3D Noise Immune Algorithm (Huntley Algorithm)

Object	Size	Proposed Algorithm	Huntley Algorithm	Cusack Algorithm
Simulated sphere	$256 \times 256 \times 100$	19.03	21.04	26.24
Simulated noisy surface	$256 \times 256 \times 100$	19.31	25.03	27.04
Mannequin's chest	$512 \times 512 \times 50$	38.39	39.34	42.86
RANDO Dummy's face	$512 \times 512 \times 50$	38.90	40.90	44.81
Real clinical patient	$512 \times 512 \times 50$	42.21	48.27	49.45

4. Conclusion

A novel three-dimensional (3D) phase unwrapping algorithm has been proposed. The proposed algorithm has been demonstrated to be very robust and computationally efficient. It relies upon a quality measure to enable unwrapping of the highest quality regions first and the lowest quality regions last, following a discrete unwrapping path.

The proposed algorithm was tested on both computer-simulated and real wrapped-phase volumes. It was found that it is capable of unwrapping very noisy objects and producing good results with a short associated computational time. The results of the proposed algorithm were also compared with two other state-of-the-art, robust, 3D phase unwrapping algorithms; the first proposed by Huntley and the second proposed by Cusack *et al*.

The advantages of the proposed algorithm can be outlined as follows:

1. The proposed algorithm utilizes a quality map to unwrap reliable regions first and leaves noisy regions to be unwrapped last in order to prevent error propagation. This is contrary to the Huntley algorithm that assigns equal qualities to all voxels, which may lead to error propagation.
2. The proposed algorithm does not rely on the quality of the voxels; it relies on the quality of the edges that connect two neighboring voxels. Depending upon edge quality to guide the unwrapping path produces better results than relying on voxel quality.
3. The proposed algorithm follows discrete unwrapping paths to ensure the processing of the highest quality regions even if they are separated from each other.

The authors acknowledge the kind assistance of Rhodri Cusack for providing a precompiled version of his phase unwrapping algorithm, which has indeed greatly helped in the success of this work.

References

1. D. C. Ghiglia and M. D. Pritt, *Two-Dimensional Phase Unwrapping: Theory, Algorithms and Software* (Wiley, 1998).
2. M. D. Pritt and J. S. Shipman, "Least-square two-dimensional phase unwrapping using FFTs," IEEE Trans. Geosci. Remote Sens. **32,** 706–708 (1994).
3. D. C. Ghiglia and L. A. Romero, "Minimum L^p-norm two-dimensional phase unwrapping," J. Opt. Soc. Am. A **13,** 1999–2013 (1996).
4. R. Cusack, J. M. Huntley, and H. T. Goldrein, "Improved noise-immune phase-unwrapping algorithm," Appl. Opt. **24,** 781–789 (1995).
5. S. A. Karout, M. A. Gdeisat, D. R. Burton, and M. J. Lalor, "Two-dimensional phase unwrapping using a hybrid genetic algorithm," Appl. Opt. **46,** 730–743 (2007).
6. M. A. Herráez, D. R. Burton, M. J. Lalor, and D. B. Clegg, "Robust, simple, and fast algorithm for phase unwrapping," Appl. Opt. **35,** 5847–5852 (1996).
7. W. Xu and I. Cumming, "A region-growing algorithm for InSAR phase unwrapping," IEEE Trans. Geosci. Remote Sens. **34,** 2044–2046 (1996).
8. M. A. Herráez, D. R. Burton, M. J. Lalor, and M. A. Gdeisat, "Fast two-dimensional phase unwrapping algorithm based on sorting by reliability following a non-continuous path," Appl. Opt. **41,** 7437–7444 (2002).
9. F. Lilley, M. J. Lalor, and D. R. Burton, "Robust fringe analysis system for human body shape measurement," Opt. Eng. **39,** 187–195 (2000).
10. M. Costanitini, F. Malvarosa, L. Minati, and G. Milillo, "A three dimensional phase unwrapping algorithm for processing of multitemproral SAR interferometric measurements," IEEE Trans. Geosci. Remote Sens. **40,** 1741–1743 (2002).
11. R. Cusack and N. Papadakis, "New robust three-dimensional phase unwrapping algorithm: application on magnetic field mapping and undistorting echo-planar images," Neuroimage **16,** 754–764 (2001).
12. X. Su, W. Chen, Q. Zhang, and Y. Chao, "Dynamic 3D-shape measurement method based on FTP," Opt. Lasers Eng. **36,** 49–64 (2001).
13. J. M. Huntley, "Three-dimensional noise-immune phase unwrapping algorithm," Appl. Opt. **40,** 3901–3908 (2001).
14. M. Jenkinson, "Fast, automated, *N*-dimensional phase unwrapping algorithm," Magn. Reson. Med. **49,** 193–197 (2003).
15. H. S. Abdul-Rahman, M. A. Gdeisat, D. R. Burton, and M. J. Lalor, "Fast three-dimensional phase unwrapping algorithm based on sorting by reliability following a non-continuous path," Proc. SPIE **5856,** 32–40 (2005).
16. H. S. Abdul-Rahman, M. A. Gdeisat, D. R. Burton, and M. J. Lalor, "Three-dimensional phase unwrapping algorithms: a comparison," presented at the Photon06 Conference, Manchester, UK, 4–7 Sept. 2006.